Biochimica et Biophysica Acta 1833 (2013) 1294–1303

Contents lists available at SciVerse ScienceDirect

Biochimica et Biophysica Acta

journal homepage: www.elsevier.com/locate/bbamcr

STIM1 participates in the contractile rhythmicity of HL-1 cells by moderating T-type Ca^{2+} channel activity

Nathalie Nguyen [a], Michael Biet [b], Élie Simard [a], Éric Béliveau [a], Nancy Francoeur [a], Gaétan Guillemette [a], Robert Dumaine [b], Michel Grandbois [a], Guylain Boulay [a,*]

[a] Department of Pharmacology, Faculty of Medicine and Health Sciences, Université de Sherbrooke, Sherbrooke, QC, Canada
[b] Department of Physiology and Biophysics, Faculty of Medicine and Health Sciences, Université de Sherbrooke, Sherbrooke, QC, Canada

ARTICLE INFO

Article history:
Received 5 October 2012
Received in revised form 11 February 2013
Accepted 20 February 2013
Available online 28 February 2013

Keywords:
STIM1
T-type calcium channel
Contractility
Ca^{2+} overload

ABSTRACT

STIM1 plays a crucial role in Ca^{2+} homeostasis, particularly in replenishing the intracellular Ca^{2+} store following its depletion. In cardiomyocytes, the Ca^{2+} content of the sarcoplasmic reticulum must be tightly controlled to sustain contractile activity. The presence of STIM1 in cardiomyocytes suggests that it may play a role in regulating the contraction of cardiomyocytes. The aim of the present study was to determine how STIM1 participates in the regulation of cardiac contractility. Atomic force microscopy revealed that knocking down STIM1 disrupts the contractility of cardiomyocyte-derived HL-1 cells. Ca^{2+} imaging also revealed that knocking down STIM1 causes irregular spontaneous Ca^{2+} oscillations in HL-1 cells. Action potential recordings further showed that knocking down STIM1 induces early and delayed afterdepolarizations. Knocking down STIM1 increased the peak amplitude and current density of T-type voltage-dependent Ca^{2+} channels (T-VDCC) and shifted the activation curve toward more negative membrane potentials in HL-1 cells. Biotinylation assays revealed that knocking down STIM1 increased T-VDCC surface expression and co-immunoprecipitation assays suggested that STIM1 directly regulates T-VDCC activity. Thus, STIM1 is a negative regulator of T-VDCC activity and maintains a constant cardiac rhythm by preventing a Ca^{2+} overload that elicits arrhythmogenic events.

1. Introduction

Ca^{2+} is central in the regulation of cardiac contractility [1]. Cardiac contractility relies on the synergic action of L-type voltage-dependent Ca^{2+} channel (L-VDCC) and cardiac ryanodine receptor (RyR2), which provide Ca^{2+} through Ca^{2+}-induced Ca^{2+} release (CICR) [2]. In addition to this essential mechanism, another process known as store-operated Ca^{2+} entry (SOCE), replenishes the sarcoplasmic reticulum (SR), the main Ca^{2+} store of the cell. This process has been best characterized in non-excitable cells, but has also been observed in excitable cells. For example, SOCE has been shown to prevent skeletal muscle fatigue by sustaining the Ca^{2+} store content of the SR [3]. SOCE has also been shown to play a role in the development of cardiomyocyte hypertrophy [4,5]. However, there is no indication as yet that SOCE is directly involved in the contractile activity of cardiomyocytes. Stromal interaction molecule 1 (STIM1) and Orai1 are the two major components of SOCE [6,7]. STIM1 is a single-pass transmembrane protein located on the SR where it serves as a Ca^{2+} sensor [8]. Upon store depletion, STIM1 detects a decrease in the SR Ca^{2+} concentration through its EF-hand domain and forms punctae that move near the plasma membrane, where it directly binds to and activates Orai1 [9–11]. Orai1 forms a tetrameric Ca^{2+} channel at the plasma membrane [12]. Orai1 is the pore-forming region of CRAC [13,14].

In cardiomyocytes, where the fluctuation of the intracellular Ca^{2+} concentration leads to rhythmic contraction, the Ca^{2+} content of the SR must be tightly controlled. Since STIM1 is expressed in HL-1 cells [15] and acts as the Ca^{2+} sensor of the SR, it should participate in the regulation of the contractile activity of cardiomyocytes. The aim of the present study was thus to determine whether STIM1 is involved in the regulation of cardiac contractility. Here, we show that knocking down STIM1 causes a deregulation of both spontaneous contractions and intracellular Ca^{2+} oscillations in HL-1 cells. Action potentials are also perturbed when STIM1 expression is decreased, eliciting arrhythmogenic events called delayed afterdepolarizations. We further show that STIM1 physically interacts with T-VDCC to prevent an increase in $I_{Ca,T}$ density and negatively modulates T-VDCC activity. This result is further confirmed by an increase in T-VDCC surface expression when STIM1 expression is decreased. Taken altogether, these results

Abbreviations: $[Ca^{2+}]_i$, concentration of intracellular free Ca^{2+}; AFM, atomic force microscopy; CICR, Ca^{2+}-induced Ca^{2+} release; CRAC, Ca^{2+}-release activated Ca^{2+} channel; I_{Ca}, Ca^{2+} current; $I_{Ca,T}$, T-type Ca^{2+} current; L-VDCC, L-type voltage-dependent calcium channel; RI, rhythmicity index; RyR2, cardiac ryanodine receptor; SERCA, sarco/endoplasmic reticulum Ca^{2+} ATPase pump; SOCE, store-operated Ca^{2+} entry; SR, sarcoplasmic reticulum; STIM1, stromal interaction molecule 1; T-VDCC, T-type voltage-dependent calcium channel; VDCC, voltage-dependent Ca^{2+} channel

* Corresponding author at: Department of Pharmacology, Faculty of Medicine and Health Sciences, Université de Sherbrooke, 3001, 12th Avenue North, Sherbrooke, QC, Canada J1H 5N4. Tel.: +1 819 820 6868x15470; fax: +1 819 564 5400.
E-mail address: Guylain.Boulay@USherbrooke.ca (G. Boulay).

0167-4889/$ – see front matter © 2013 Elsevier B.V. All rights reserved.
http://dx.doi.org/10.1016/j.bbamcr.2013.02.027

show that STIM1 plays a key role in controlling the heart rhythm by moderating T-VDCC activity.

2. Materials and methods

2.1. Materials

Claycomb medium, fetal bovine serum (FBS), ascorbic acid, norepinephrine (NE), soybean trypsin inhibitor, fibronectin, and caffeine were purchased from Sigma-Aldrich (St. Louis, MO, USA). Trypsin-EDTA 0.05% was from Wisent Inc. (St-Bruno, QC, Canada). Penicillin/streptomycin, L-glutamine, Hepes, Lipofectamine 2000, OptiMEM, and Block-it AlexaFluor Red Fluorescent Oligo were from Invitrogen (Burlington, ON, Canada). Fura-2/AM was from Calbiochem (La Jolla, CA, USA). Rabbit polyclonal anti-STIM1 antibody, mouse monoclonal anti-actin antibody, and nitrocellulose membranes were from Millipore (Temecula, CA, USA). Rabbit polyclonal anti-STIM2 antibody was from AbCam (Cambridge, MA, USA). Rabbit polyclonal anti-$Ca_V3.1$ antibody was from Alomone Labs (Jerusalem, Israel). Horseradish peroxidase-conjugated sheep anti-mouse and horseradish peroxidase-conjugated donkey anti-rabbit antibodies were from Amersham Biosciences. A/G PLUS-agarose beads were from Santa Cruz Biotechnology (Santa Cruz, CA, USA). Sulfo-NHS-SS-Biotin and streptavidin-agarose beads were from Pierce (Pierce Biotechnology, Rockford, IL, USA). STIM1 siRNA and control siRNA (ON-TARGETplus Control Pool) were from Dharmacon, Inc. (Lafayette, CO, USA). Unless otherwise stated, all other reagents were from Sigma-Aldrich (Oakville, ON, Canada) or Laboratoire MAT (Quebec City, QC, Canada).

2.2. Cell culture and transfection with siRNAs

The cardiomyocyte-derived HL-1 cell was used because it displays spontaneous and rhythmic activities (contractions, Ca^{2+} oscillations and electrical activity) and can be easily manipulated to gain a better understanding of these activities at the cellular and molecular levels. HL-1 cell line was kindly provided by William Claycomb (Louisiana State University Medical Center, New Orleans, LA, USA) and was cultured as previously described [16]. Briefly, HL-1 cells were cultured in Claycomb medium supplemented with 10% FBS in the presence of 2 mM L-glutamine, 100 μg/mL streptomycin, 100 U/mL penicillin, and 100 μM NE (prepared from a 10 mM stock solution in 30 mM ascorbic acid) at 37 °C in a humidified 5% CO_2 environment. HL-1 cells were transiently transfected with siRNAs at a final concentration of 50 nM using Lipofectamine 2000 according to manufacturer's instructions. siRNA transfection efficiency and the selection of transfected cells for $[Ca^{2+}]_i$ and contraction measurements were assessed using Block-it AlexaFluor Red Fluorescent Oligo. siRNA transfection efficiency was approximately 90%.

2.3. Co-immunoprecipitation and Western blotting

HL-1 cells were lysed with cold RIPA buffer containing 20 mM Tris-HCl (pH 8.0), 150 mM NaCl, 1% Nonidet P40, 0.5% deoxycholate, 5 mM EDTA, 0.1% SDS, 1 μg/mL soybean trypsin inhibitor, 5 μg/mL leupeptin, and 100 μM phenylmethylsulfonyl fluoride for 20 min at 4 °C followed by 20 passages through a 20-gauge needle and 5 passages through a 25-gauge needle. The cell lysate was centrifuged at 15,000 g for 15 min to remove insoluble materials, and the protein concentration in the supernatant was determined using the Bradford method. The supernatant was then incubated for 16 h at 4 °C with the indicated antibody immobilized on protein A/G PLUS-agarose beads. The beads were washed three times with solubilizing buffer and were heated for 30 min at 60 °C in 2× Laemmli buffer containing 40 mg/mL of dithiothreitol to denature the proteins. The proteins were then resolved by SDS-PAGE and were transferred to nitrocellulose membranes in a buffer containing 25 mM Tris-base, 200 mM glycine, and 20% methanol (pH ~8.2). After staining with Ponceau S, the blots were washed with TBS-T and were incubated for 1 h at room temperature in 5% non-fat skim milk. To detect protein bands, the blots were incubated with the indicated antibodies for 16 h at 4 °C followed by HRP-coupled anti-antibodies for 90 min at room temperature, and then with an enhanced chemiluminescence reagent.

2.4. Biotinylation of cell surface proteins

To biotinylate cell surface proteins, we used the method described by Cayouette et al. [17]. Briefly, siRNA-transfected HL-1 cells grown for 48–72 h in 6-well plates were washed with ice-cold PBS containing 0.9 mM $CaCl_2$ and 1 mM $MgCl_2$ (PBS with Ca^{2+}/Mg^{2+}). The cells were placed on ice and washed twice with ice-cold PBS and then incubated for 90 min at 4 °C with 3 mg/mL of Sulfo-NHS-SS-Biotin in PBS with Ca^{2+}/Mg^{2+}. The biotinylation reaction was terminated by washing the cells three times with ice-cold PBS containing 10 mM glycine. The cells were then lysed with 400 μL of ice-cold RIPA buffer for 30 min at 4 °C followed by 20 passages through a 20-gauge needle and 5 passages through a 25-gauge needle. The cell extracts were cleared by centrifugation and added to 75 μL of streptavidin-agarose beads and incubated for 16 h at 4 °C. The biotin-streptavidin-agarose complexes were harvested by centrifugation and washed three times with RIPA buffer. The beads were then resuspended in 2× Laemmli buffer containing 40 mg/mL of dithiothreitol and incubated at 60 °C for 30 min before SDS-PAGE separation and immunoblotting.

2.5. Measurement of intracellular free Ca^{2+}, $[Ca^{2+}]_i$

The method described by Zhu et al. was used to measure $[Ca^{2+}]_i$ [18]. Briefly, HL-1 cells were grown on coverslips pre-coated with gelatin/fibronectin. After a 48–72 h transfection, the coverslips were washed twice with Hepes buffered saline solution (HBSS (in mM): 120 NaCl, 5.3 KCl, 0.8 $MgSO_4$, 10 glucose, 1.8 $CaCl_2$, 20 Hepes, pH 7.4) and were loaded with fura-2/AM (4 μM in HBSS) for 20 min at room temperature in the dark. After washing and de-esterifying in fresh HBSS for 20 min at room temperature, the coverslips were inserted in a circular open-bottom chamber and were placed on the stage of an Olympus IX71 microscope (Olympus Canada Inc., Markham, ON, Canada) equipped with a Lambda-DG-4 illuminator (Sutter Instrument Company, Novato, CA, USA). $[Ca^{2+}]_i$ in selected fura2-loaded cells (40 to 50 cells/coverslip) was measured by fluorescence videomicroscopy at room temperature using alternating excitation wavelengths of 340 nm (26 nm bandpass) and 387 nm (11 nm bandpass). Emitted fluorescence was monitored at 510 nm (84 nm bandpass) through a 415–570 nm dichroic mirror. Fluorescence intensity was monitored using an Evolve™ EMCCD camera (Photometrics, Tucson, AZ, USA). The images were digitized and analyzed using MetaFluor software (Universal Imaging Corporation, Downingtown, PA, USA). Free $[Ca^{2+}]_i$ was calculated from the 340/387 fluorescence ratios using the method of Grynkiewicz et al. [19]. All reagents were diluted to their final concentrations in HBSS and were applied to the cells by surface perfusion. Ca^{2+}-free HBSS was supplemented with 0.5 mM EGTA to chelate any remaining extracellular Ca^{2+}.

2.6. Measurement of contractility by atomic force microscopy (AFM)

The method described by Domke et al. was used to measure HL-1 cells contractility [20]. Briefly, cells were grown on 60-mm-diameter dishes pre-coated with gelatin/fibronectin. After a 48–72 h transfection, the dishes were placed in a custom-made AFM setup mounted over an inverted microscope (Motic, Richmond, BC, Canada), which made it possible to observe beating cells and position the AFM tip on top of them. The system was comprised of a Z-piezo scanner (P753.21C,

Physik Instrumente, Auburn, MA, USA) equipped with a capacitive sensor with a nominal closed-loop resolution of 0.1 nm, a piezoelectric XY positioner (PXY 200/28 motion x, y 200 μM, Piezosystem Jena, MA, USA), and a 635-nm laser source (OZ-2000 series, OZ Optics, USA) to detect cantilever deflection. The setup was installed in an acoustic and vibration isolation box at a controlled temperature at 37 °C. All experiments were performed with non-conductive silicon nitride cantilevers (Veeco, Camarillo, CA, USA), with a nominal force constant of 0.01 N/m, calibrated using the thermal noise method [21,22]. Data was analyzed using Igor Pro WaveMetrics software (Lake Oswego, OR, USA).

2.7. Electrophysiology

Action potentials were recorded at room temperature using the current clamp technique. The extracellular solution contained (in mM): 120 NaCl, 5.3 KCl, 0.8 $MgSO_4$, 10 glucose, 1.8 $CaCl_2$, and 20 Hepes (pH 7.4 adjusted with NaOH). The pipette solution contained (in mM): 120 K-aspartate, 25 KCl, 1 $MgCl_2$, 10 EGTA, 2 Na_2phosphocreatine, 4 Na_2ATP, 2 Na_2GTP, and 5 Hepes (pH 7.2 adjusted with KOH). The whole cell patch clamp technique was used to record Ca^{2+} currents (I_{Ca}). HL-1 cells were dissociated in 0.05% trypsin-EDTA for 5 min. The digestion reaction was stopped using 0.025% soybean trypsin inhibitor. Data were acquired at room temperature using an Axopatch 200B amplifier equipped with a CV-201A head stage (Axon Instruments, Foster City, CA, USA). During recordings, the cells were perfused with a bath solution containing (in mM): 140 TEACl, 2 $MgCl_2$, 5 $CaCl_2$, 10 glucose, and 10 Hepes (pH 7.4 adjusted with CsOH). Patch pipette resistance was between 2 and 4 MΩ when filled with a solution containing (in mM) 100 CsCl, 20 TEACl, 10 EGTA, 10 Hepes, 3 Na_2ATP, and 0.5 Na_2GTP (pH 7.2 adjusted with CsOH). All solutions were adjusted to 290 mOsm with sucrose. Data were acquired and analyzed using pCLAMP (Molecular Devices Inc., Sunnyvale, CA, USA) and Origin software (OriginLab Corporation, Northampton, MA, USA).

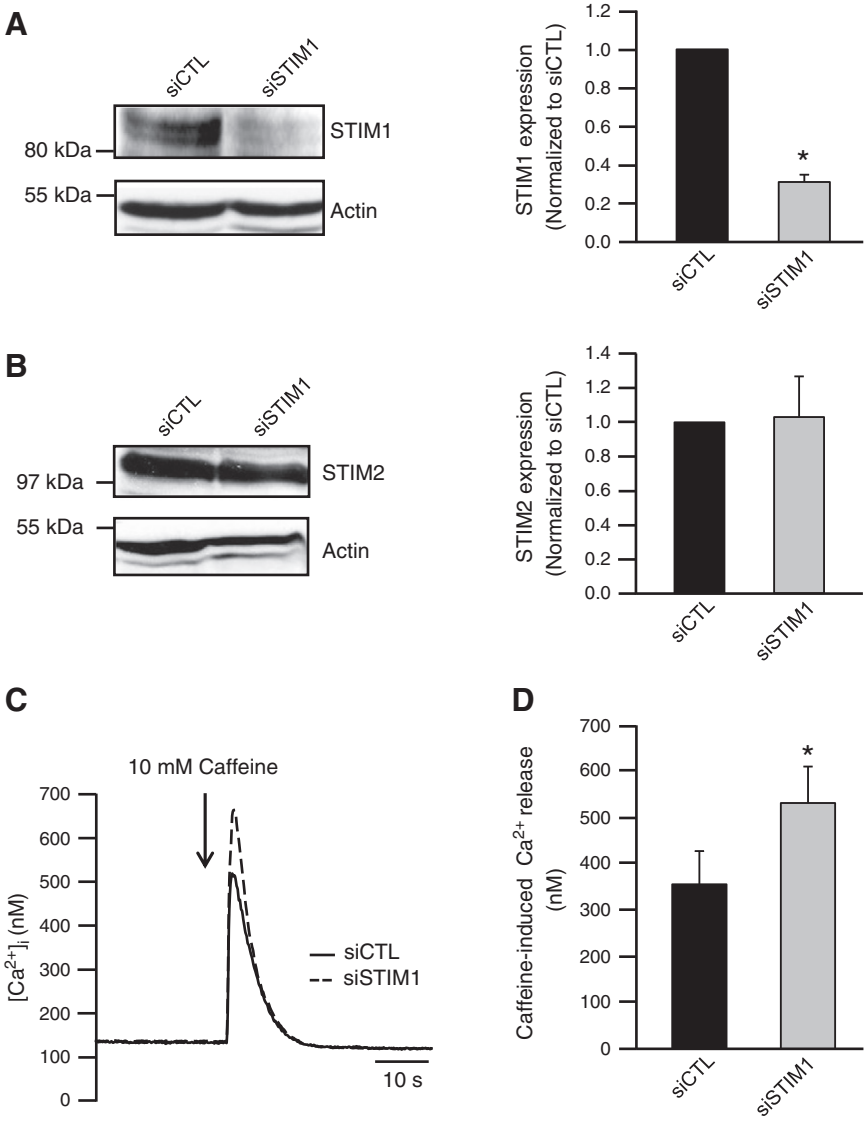

Fig. 1. STIM1 is expressed and controls the ryanodine-sensitive Ca^{2+} pool in HL-1 cells. (A, B) Cells were transfected with 50 nM of control siRNA or siSTIM1. After 48–72 h, cells were lysed and proteins were resolved by SDS-PAGE, and identified by Western blot using anti-STIM1 (A), anti-STIM2 (B) or anti-actin antibodies. Bar graphs show averaged data of the densitometric analysis (n = 3 independent experiments). (C) Average traces showing caffeine-induced Ca^{2+} releases in HL-1 cells bathed in a Ca^{2+} free medium. (D) Summarized data showing caffeine-induced Ca^{2+} release in control cells (n = 8 coverslips with 40–50 cells/coverslip) and in cells transfected with siSTIM1 (n = 6 coverslips with 40–50 cells/coverslip). *P < 0.05 with an unpaired Student's *t* test.

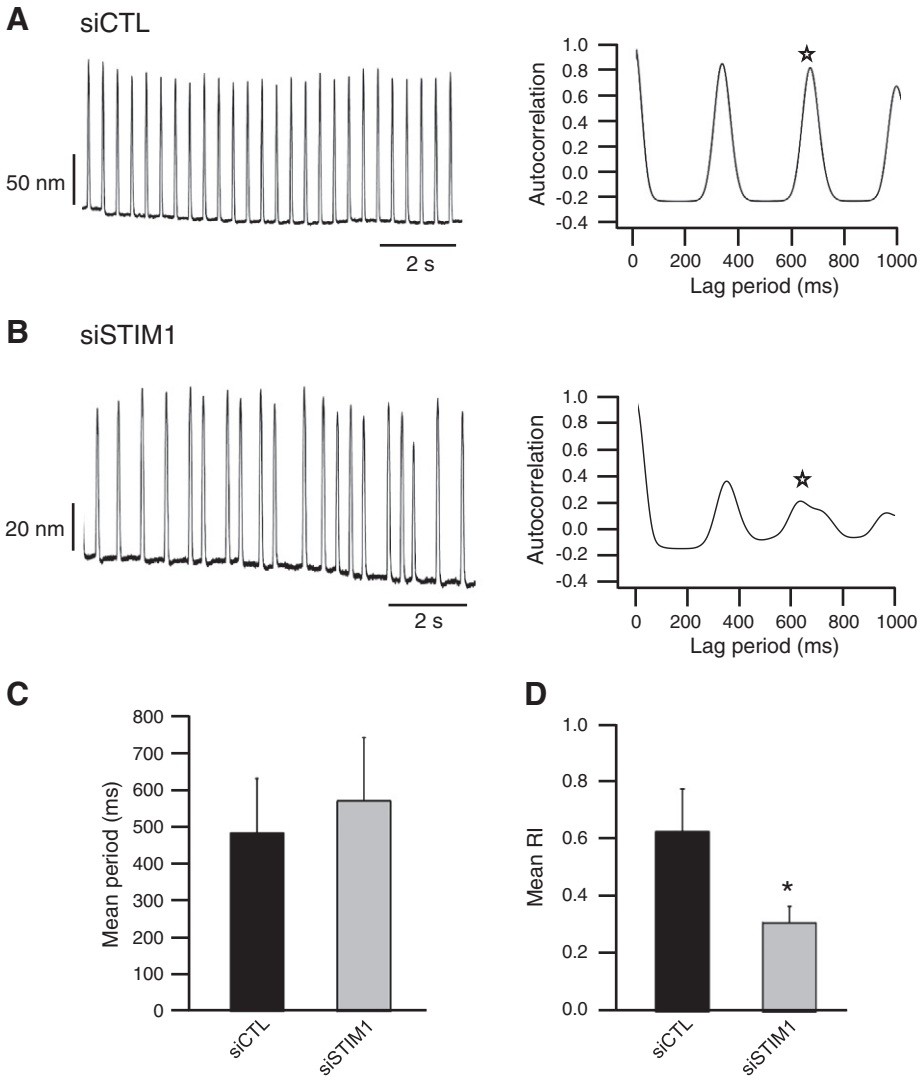

Fig. 2. Knocking down STIM1 perturbs the rate of contraction of HL-1 cells. (A) Representative trace showing the contraction of a cell transfected with siCTL and the corresponding autocorrelation analysis. (B) Representative trace showing the contraction of a cell transfected with siSTIM1 and the corresponding autocorrelation analysis. The stars indicate the rhythmicity index (RI) value for each trace. (C, D) Summarized data showing the mean contraction periods (C) and the mean RI (D) in control cells (n = 37 cells) and in cells transfected with siSTIM1 (n = 35 cells). *P < 0.05 with an unpaired Student's *t* test.

2.8. Statistical analysis

All values are expressed as means ± S.D., and statistical significance was tested using an unpaired Student's *t*-test. $P \leq 0.05$ was considered statistically significant. The mean periods and rhythmicity index (RI) were determined for each cell using an autocorrelation analysis as described by Levine et al. [23] with the Perl Statistics-Autocorrelation module (http://www.cpan.org) or ClampFit program (Molecular Devices Inc., Sunnyvale, CA, USA). The RI has been previously used to describe rhythm strength in studies on rhythmic Ca^{2+} oscillations in cardiac pacemaker cells [24].

3. Results

3.1. STIM1 is expressed and controls the ryanodine-sensitive Ca^{2+} pool in HL-1 cells

The involvement of endogenous STIM1 in the cellular Ca^{2+} homeostasis of HL-1 cells was investigated by silencing its expression with an siRNA specific for STIM1 mRNA. Fig. 1A shows that STIM1 is expressed in HL-1 cells. The transfection of HL-1 cells with an siRNA specific for STIM1 (siSTIM1) decreased its expression to 31.2 ± 3.7% of that of cells transfected with a control siRNA (siCTL) (Fig. 1A). The expression of STIM2, a closely related family member, was unaffected by the transfection of siSTIM1 (Fig. 1B). Since STIM1 is known to be an SR Ca^{2+} sensor, we first investigated whether knocking down STIM1 would affect the intracellular Ca^{2+} store of HL-1 cells. The Ca^{2+} content of the SR was evaluated by releasing the ryanodine-sensitive Ca^{2+} pool using 10 mM caffeine in the absence of extracellular Ca^{2+}. Fig. 1C shows mean traces of caffeine-induced Ca^{2+} release in cells transfected with siCTL (solid line) or siSTIM1 (dashed line). Caffeine-induced Ca^{2+} release was significantly higher in siSTIM1-transfected cells (527 ± 78 nM) than in control cells (353 ± 72 nM) (Fig. 1D). We verified that the transfection of an unspecific siRNA did not affect the caffeine-induced Ca^{2+} release in HL-1 cells (see Supplemental data Fig. 1). These results suggested that knocking down STIM1 in HL-1 cells increases the ryanodine-sensitive Ca^{2+} pool of the SR.

3.2. Knocking down STIM1 perturbs the rate of contraction of HL-1 cells

The effect of STIM1 knockdown on the contractility of HL-1 cells was evaluated using AFM in its force measurement mode. In this experiment, the rhythmic contractions of a cluster of cells were

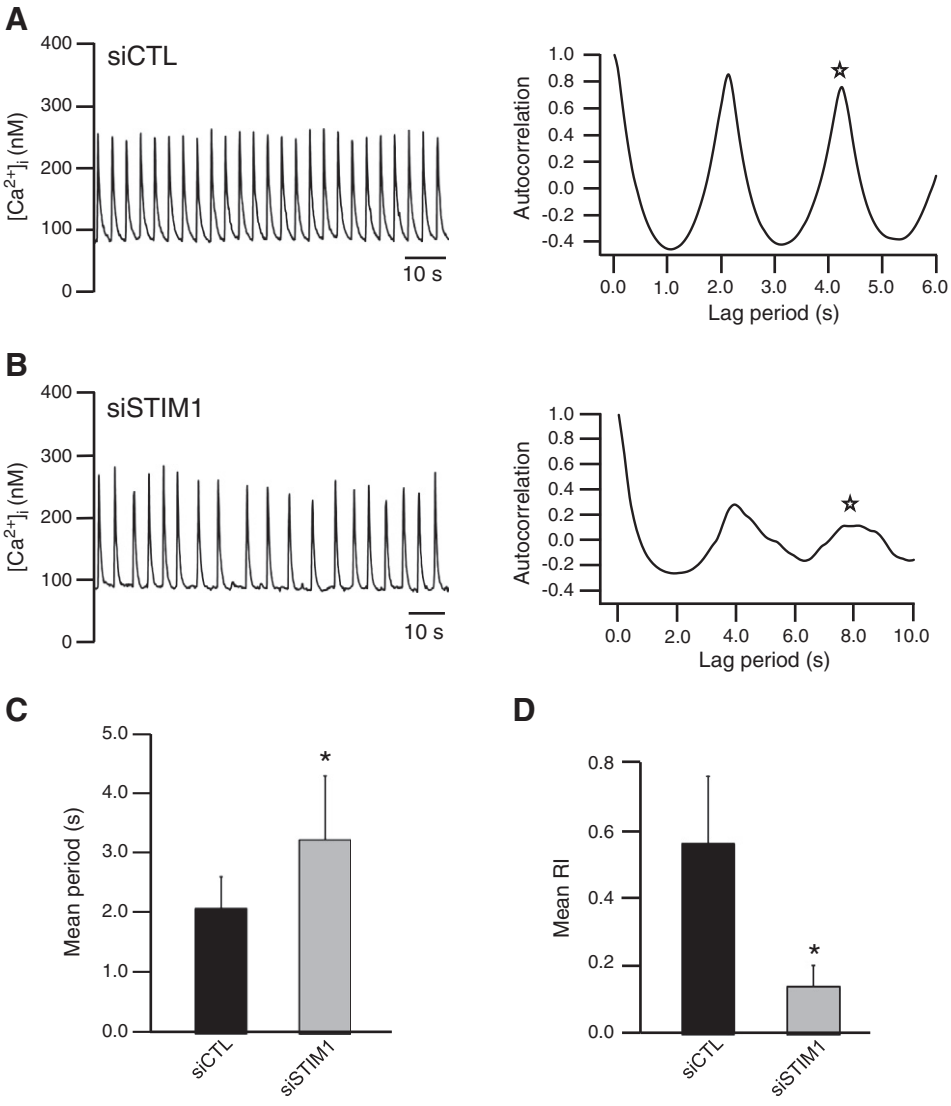

Fig. 3. Knocking down STIM1 causes irregular spontaneous Ca^{2+} oscillations in HL-1 cells. (A) Representative trace showing spontaneous Ca^{2+} oscillations in a control cell and the corresponding autocorrelation analysis. (B) Representative trace showing spontaneous Ca^{2+} oscillations in a cell transfected with siSTIM1 and the corresponding autocorrelation analysis. The stars indicate the rhythmicity index (RI) value for each trace. (C, D) Summarized data showing the mean Ca^{2+} oscillation periods (C) and the mean RI (D) in control cells (n = 214 cells) and in cells transfected with siSTIM1 (n = 335 cells). *P < 0.05 with an unpaired Student's *t* test.

detected by recording the deflection of the cantilever (in nm) as a function of time [20]. Fig. 2A shows typical contractions of HL-1 cells transfected with siCTL and the autocorrelation analysis of the typical trace. The contraction signal was regular, with a mean period of 483 ± 147 ms (Fig. 2C). Fig. 2B shows typical contractions of HL-1 cells transfected with siSTIM1 and the corresponding autocorrelation analysis. Interestingly, the contraction signal was visually more irregular than control cells and yielded a mean period of 569 ± 171 ms (Fig. 2C). The mean RI (which reflects the strength of rhythmicity and is identified as the third peak on the correlogram) [23] was significantly lower in HL-1 cells transfected with siSTIM1 (0.31 ± 0.06) than in cells transfected with siCTL (0.63 ± 0.15) (Fig. 2D). We verified that the transfection of an unspecific siRNA did not affect the contractions of HL-1 cells (see Supplemental data Fig. 2A-C). These results showed that STIM1 is involved in the control of contraction rhythmicity in HL-1 cells.

3.3. Knocking down STIM1 induces irregular spontaneous Ca^{2+} oscillations in HL-1 cells

HL-1 cells display spontaneous Ca^{2+} oscillations under basal conditions [16,25]. Since Ca^{2+} is the key component underlying each contraction, the effect of knocking down STIM1 on spontaneous Ca^{2+} oscillations in HL-1 cells was evaluated. Fig. 3A shows typical Ca^{2+} oscillations in a cell transfected with siCTL and the autocorrelation analysis of the corresponding trace. The mean period of the Ca^{2+} oscillations in control cells was 2.1 ± 0.5 s (Fig. 3C) and the mean RI was 0.57 ± 0.20 (Fig. 3D). Fig. 3B shows typical Ca^{2+} oscillations in a cell transfected with siSTIM1 and the corresponding autocorrelation analysis. Knocking down STIM1 slowed the Ca^{2+} oscillations to a mean period of 3.2 ± 1.1 s (Fig. 3C). The rhythm became also more irregular, with a mean RI of 0.14 ± 0.06 (Fig. 3D). We also verified that the transfection of an unspecific siRNA did not affect Ca^{2+} oscillations in HL-1 cells (see Supplemental data Fig. 2D-F). These results showed that STIM1 is involved in the rhythmicity of spontaneous Ca^{2+} oscillations in HL-1 cells.

3.4. Knocking down STIM1 increases $I_{Ca,T}$ density and alters electrical excitability

The perturbed rhythmicity of spontaneous Ca^{2+} oscillations may influence the duration and the waveform of action potentials in HL-1 cells. We thus investigated the effect of knocking down STIM1

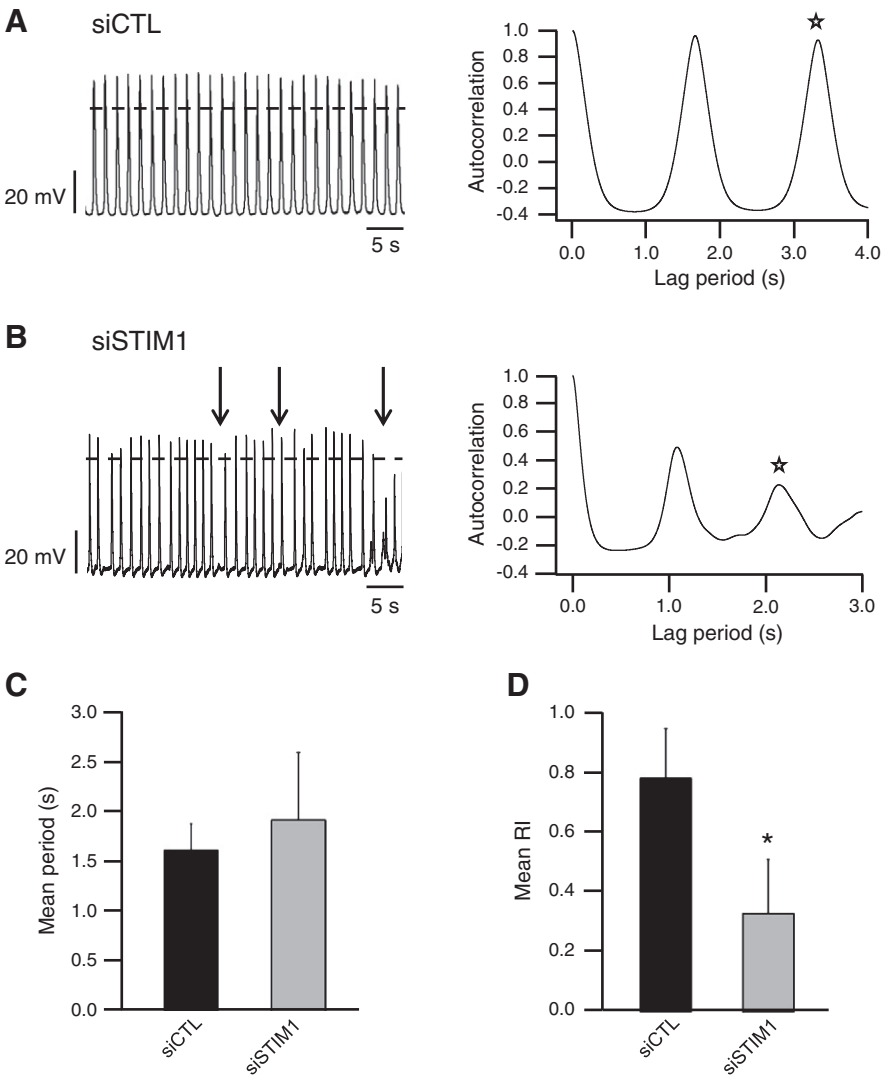

Fig. 4. Knocking down STIM1 induces arrhythmogenic events in HL-1 cells. (A) Action potentials recorded in a typical cell transfected with siCTL and the corresponding autocorrelation analysis. Similar results were obtained with all of the 6 cells tested. (B) Action potentials recorded in a typical cell transfected with siSTIM1 and the corresponding autocorrelation analysis. Similar results were obtained with 5 out of 8 cells tested, reflecting a residual expression of STIM1 after its knockdown. The dashed line corresponds to 0 mV on action potential recordings. The arrows indicate arrhythmogenic events and the stars indicate the rhythmicity index (RI) value for each trace. (C, D) Summarized data showing the mean action potential periods (C) and the mean RI (D) in control cells (n = 6 cells) and in cells transfected with siSTIM1 (n = 8 cells). *P < 0.05 with an unpaired Student's *t* test.

on action potentials of HL-1 cells. Fig. 4A shows typical and regular action potentials in control cells. The mean period was 1.6 ± 0.3 s and the mean RI was 0.79 ± 0.17 (Fig. 4C and D). In cells transfected with siSTIM1, arrhythmogenic events such as delayed afterdepolarizations were observed (as indicated by arrows in Fig. 4B). In these cells, the mean period was 1.9 ± 0.7 s and the mean RI was 0.33 ± 0.18 (Fig. 4C and D). The presence of delayed afterdepolarizations is consistent with the increased ryanodine-sensitive Ca^{2+} pool observed in Fig. 1C and D and indicates an SR Ca^{2+} overload.

To gain further insights into the molecular mechanism that is perturbed when STIM1 is knocked down in HL-1 cells, we investigated the electrophysiological properties of VDCC. I_{Ca} was elicited by consecutive 300-ms test pulses between −75 and +20 mV in 5-mV increments. Under these conditions, we recorded both Ca^{2+} currents: $I_{Ca,L}$ and $I_{Ca,T}$. However, $I_{Ca,L}$ was present in only 15% of the cells used for recordings, while $I_{Ca,T}$ was the predominant Ca^{2+} current in these cells, which is consistent with previous data from Xia et al. [26]. In cells transfected with siCTL, the $I_{Ca,T}$ activation threshold was −55 mV, with a maximum peak current at −20 mV (Fig. 5A and B). In cells transfected with siSTIM1, the $I_{Ca,T}$ activation threshold was −60 mV, and the maximum peak current was reached at −25 mV. However, the peak $I_{Ca,T}$ density was 25% higher in cells transfected with siSTIM1 (−16.9 ± 2.0 pA/pF) than in control cells (−12.7 ± 1.5 pA/pF) (Fig. 5B). To obtain the voltage dependence of activation, we normalized the conductance (G) of the current at each potential to the maximal conductance (G_{max}) obtained from the slope of a linear regression fit to the linear portion of the I/V relationship. Fig. 5C shows that knocking down STIM1 significantly shifted the activation curve of $I_{Ca,T}$ toward more negative potentials, indicating that the current activates at more hyperpolarized potentials. The mean values of half-activation potential ($V_{1/2}$) were −33.4 ± 0.2 mV and −39.0 ± 0.2 mV for control cells and cells transfected with siSTIM1, respectively.

To further investigate the mechanism involved in the increased $I_{Ca,T}$ density following STIM1 knockdown, we measured the availability of T-VDCC at different voltages (steady-state inactivation). $I_{Ca,T}$ inactivation was evaluated by using the standard two-pulse protocol consisting of 300-ms preconditioning pulses between −90 and −25 mV in 5-mV increments, followed by a test pulse to +10 mV (as described in Fig. 5D). The inactivation curves of control and siSTIM1 cells (Fig. 5E) were identical, indicating that knocking down STIM1 did not affect the availability of T-VDCC. The mean values of half-inactivation potential were −49.3 ± 0.1 mV for control cells and −49.5 ± 0.2 mV

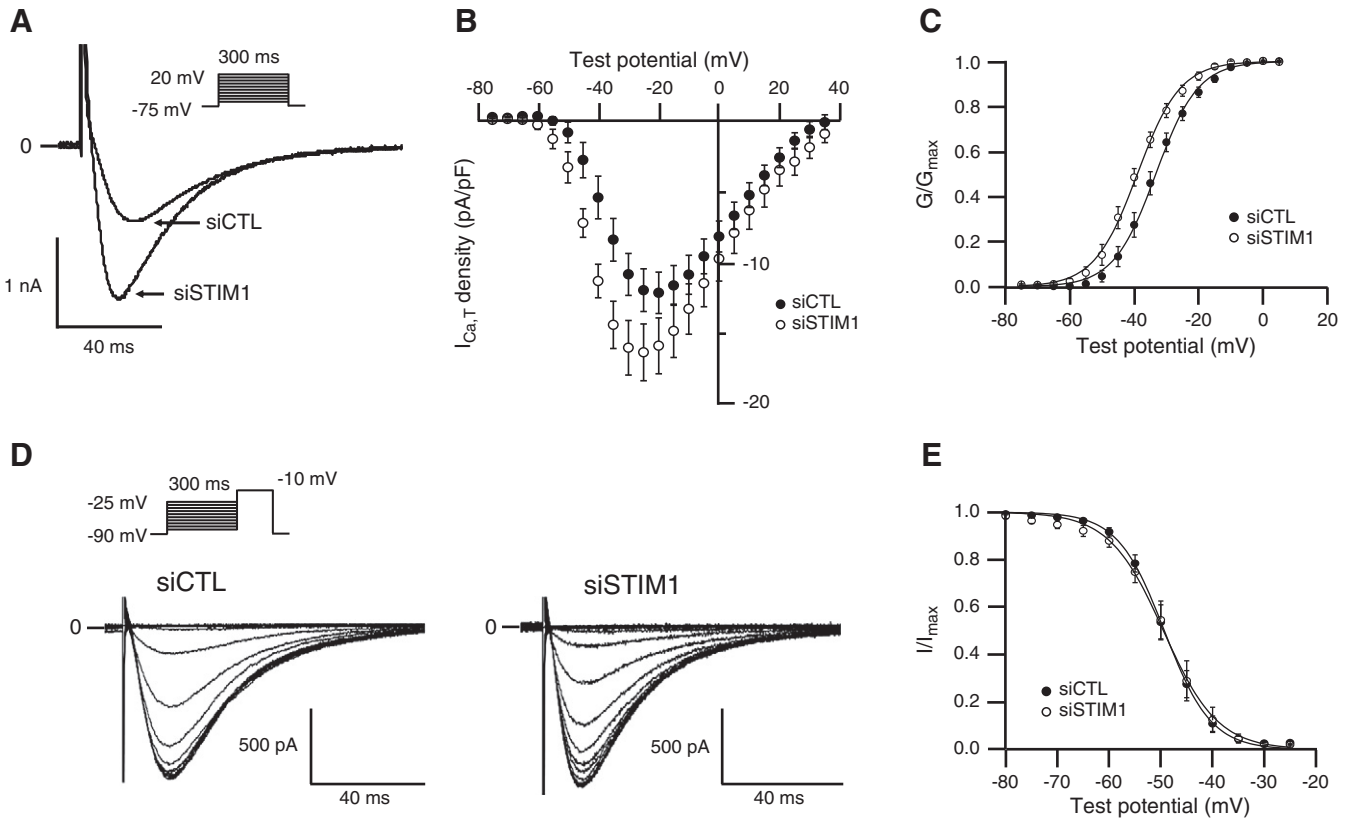

Fig. 5. Knocking down STIM1 increases $I_{Ca,T}$ density and alters electrical excitability. (A) Superimposed current traces for control cells or cells transfected with siSTIM1 at a voltage step corresponding to peak current density for each condition. (B) Averaged current-voltage relations of $I_{Ca,T}$ density in control cells (filled circles, n = 9) or cells transfected with siSTIM1 (open circles, n = 8). (C) Voltage-dependent activation curve for $I_{Ca,T}$ in control cells (filled circles, n = 9) or in cells transfected with siSTIM1 (open circles, n = 8). Data were fitted to a Boltzmann distribution using the formulation: $m_\infty = 1 / \{1 + \exp[(V_{1/2} - V) / k]\}$, where $V_{1/2}$ is the potential at which the conductance is half maximally activated and k is the slope factor describing the steepness of the curve (solid line). (D) Representative current recordings used to determine voltage dependence of $I_{Ca,T}$ inactivation for control cells or cells transfected with siSTIM1. (E) Voltage-dependent inactivation curve for $I_{Ca,T}$ in control cells (filled circles, n = 7) or in cells transfected with siSTIM1 (open circles, n = 6). Data were fitted to a Boltzmann distribution function: $h_\infty = (1) / \{1 + \exp[(V - V_{1/2}) / k]\}$, where $V_{1/2}$ is the potential at half-maximal inactivation, k is the slope factor, h_∞ represents the fraction of inactivated channels for a given voltage.

for cells transfected with siSTIM1. This result suggested that the increase in $I_{Ca,T}$ density is due to an increased expression of T-VDCC rather than changes in its availability. Altogether, these results showed that STIM1 negatively modulates T-VDCC channel activity.

3.5. Knocking down STIM1 increases $I_{Ca,T}$ window current

The overlap between the $I_{Ca,T}$ steady-state activation and inactivation curves delimits a region called "window current". In this region, the channel population dynamically equilibrates among closed, open, and inactivated states, resulting in a steady-state leak current [27]. We hypothesized that an increase in the Ca^{2+} window current following STIM1 knockdown may be involved in the SR Ca^{2+} overload. We found that the negative shift in the activation curve observed in cells transfected with siSTIM1 substantially increased the $I_{Ca,T}$ window current, which provides support for this hypothesis (Fig. 6A). The $I_{Ca,T}$ window current (I^w) was obtained by multiplying the conductance of the current (G_{max}) at any given electromotive force ($V\text{-}E_{Ca}$) by the activation and inactivation mid-potentials ($h_\infty \cdot m_\infty$) using the Hodgkin and Huxley equation: $G_{max} \cdot h_\infty \cdot m_\infty \cdot (V - E_{rev})$ [28]. Fig. 6B shows that I^w increased 3-fold in cells transfected with siSTIM1 (open circles) compared to control cells (full circles). These results were consistent with an increase in the $I_{Ca,T}$ leak (window) current contributing to a Ca^{2+} overload in siSTIM1 cells. It also indicated that STIM1 contributes to the regulation of SR Ca^{2+} loading indirectly by modulating the activity of T-type calcium channels.

3.6. Knocking down STIM1 increases T-VDCC surface expression

To determine whether the increase in T-VDCC activity was due to an increase in T-VDCC surface expression, we verified the effect of STIM1 knockdown on $Ca_V3.1$ levels, a T-VDCC isoform expressed at the plasma membrane of HL-1 cells [26,29]. Cell surface proteins were selectively biotinylated with the membrane-impermeable amino reagent sulfo-NHS-SS-biotin. The proteins were then solubilized and incubated with streptavidin-agarose beads before immunoblotting with an anti-$Ca_V3.1$ antibody. Fig. 6C shows that surface expression of $Ca_V3.1$ was increased by 1.8 ± 0.4 fold (n = 3 independent experiments) when STIM1 expression was decreased. Since the total expression of $Ca_V3.1$ was unchanged, this result suggests a redistribution of $Ca_V3.1$ from an intracellular compartment to the cell surface. This result is in agreement with our previous data showing that STIM1 negatively regulates T-VDCC activity by preventing the surface expression of the channel.

3.7. STIM1 interacts with $Ca_V3.1$ in HL-1 cells

We performed a co-immunoprecipitation assay to verify whether STIM1 physically interacts with $Ca_V3.1$. Fig. 6D shows that STIM1 was detected in the immunoprecipitate of $Ca_V3.1$ and inversely, $Ca_V3.1$ was detected in the immunoprecipitate of STIM1. On the other hand, STIM1 or $Ca_V3.1$ were not detected in the immunoprecipitate when an unrelated rabbit anti-IgG antibody (negative control) was used. These results suggested that STIM1 physically interacts with T-VDCC.

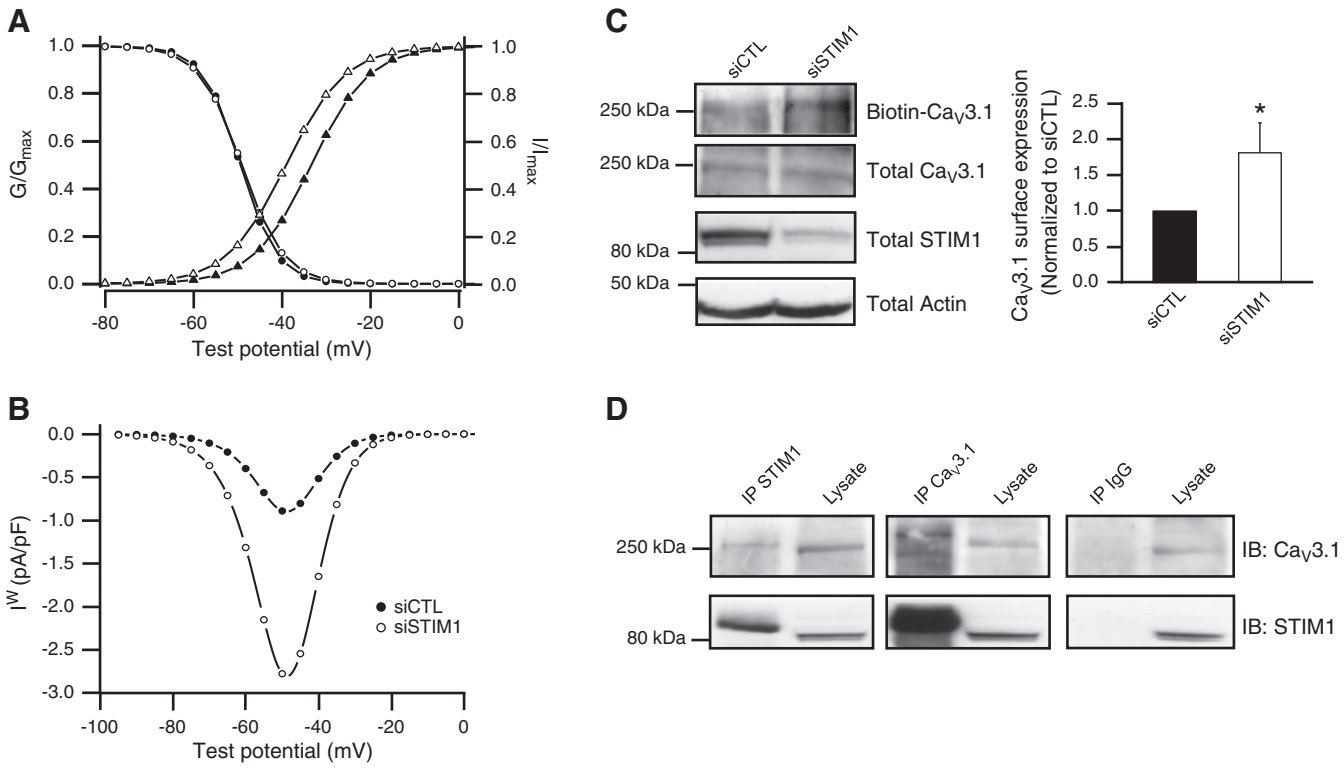

Fig. 6. Knocking down STIM1 increases $I_{Ca,T}$ window current (I^W) and T-VDCC cell surface expression. (A) Superimposed voltage-dependent activation and inactivation curves for $I_{Ca,T}$ in control cells (filled circles and triangles) or in cells transfected with siSTIM1 (open circles and triangles). The curves are fitted according to the Boltzmann equation. (B) Voltage-dependent window current for $I_{Ca,T}$ in control cells (filled circles) or in cells transfected with siSTIM1 (open circles). (C) HL-1 cells were transfected with 50 nM of control siRNA or siSTIM1. After 48–72 h, cells were biotinylated with sulfo-NHS-SS-biotin, lysed and incubated with streptavidin-agarose beads as described in the Materials and methods section. Proteins precipitated on streptavidin-agarose beads were separated by SDS-PAGE and detected with an anti-$Ca_V3.1$ antibody. Aliquots of the cell lysates were collected before incubation with streptavidin-agarose beads and analyzed directly by immunoblotting to determine the total amount of T-VDCC, STIM1 and actin in the samples. Bar graphs show averaged data of the densitometric analysis (n = 3 independent experiments). (D) Co-immunoprecipitation of STIM1 and T-VDCC (n = at least 6 independent experiments). HL-1 cells were lysed and proteins were immunoprecipitated (IP) with anti-$Ca_V3.1$, anti-STIM1 or anti-IgG antibodies, resolved by SDS-PAGE, and identified by Western blot (IB) using anti-$Ca_V3.1$ or anti-STIM1 antibodies.

4. Discussion

The aim of the present study was to investigate the involvement of STIM1 in the regulation of cardiac contractility. Our results showed that STIM1 is expressed in HL-1 cells, a murine atrial-derived cell line that displays spontaneous Ca^{2+} oscillations and contractions [16,25]. Recent reports have also shown that STIM1 is expressed in HL-1 cells [15] and other types of cardiomyocytes [4,5,30,31]. These studies have focused on the essential role of STIM1 in the Ca^{2+}-dependent development of cardiac hypertrophy. However, the role of STIM1 in the spontaneous activity and the contractile function of cardiomyocytes are unknown. In non-excitable cells, STIM1 normally acts as an activator of Orai1 and some TRPC channels when the Ca^{2+} store is depleted [32–34]. A knockdown of STIM1 results in a decrease in SOCE [6,8]. However, our results pointed to an unexpected function of STIM1 in HL-1 cells. Indeed, we showed that STIM1 dampens the activity of T-VDCC to prevent an excessive Ca^{2+} entry resulting in an SR Ca^{2+} overload that can lead to arrhythmogenic events. This is a new regulation pathway for the control of Ca^{2+} homeostasis leading to rhythmic contractions in beating HL-1 cells. These findings were further confirmed by our observation that knocking down STIM1 induces arrhythmogenic events such as delayed afterdepolarizations, which are known to occur under conditions of SR Ca^{2+} overload [35,36]. The increase in the caffeine-induced Ca^{2+} release observed in cells transfected with siSTIM1 was also consistent with an SR Ca^{2+} overload. At rest, the SR Ca^{2+} content depends on the balance between Ca^{2+} uptake by the SERCA pump and efflux of Ca^{2+} mostly through cardiac ryanodine receptors (RyR2). The activity of SERCA depends on various factors such as the $[Ca^{2+}]_i$. A higher $[Ca^{2+}]_i$ will enhance the activity of SERCA [37]. We showed that the activity of T-VDCC is enhanced in STIM1-knocked down cells, causing a greater Ca^{2+} influx into the cells. Under this circumstance, we expect that the SERCA pump activity would also be increased resulting in an excess of Ca^{2+} in the SR. A Ca^{2+} overload usually gives rise to spontaneous SR Ca^{2+} release through the RyR2, often referred to as Ca^{2+} sparks [38]. Ca^{2+} sparks participate in the initiation and propagation of Ca^{2+} waves in cardiomyocytes, ultimately leading to the extrusion of Ca^{2+} via the Na^+/Ca^{2+} exchanger and the generation of a transient inward current that can lead to early and delayed afterdepolarizations [39,40]. Importantly, it is well established that T-VDCC participates in the cardiac automaticity of pacemaker and latent pacemaker cells [41,42]. In HL-1 cells, spontaneous activity has been attributed to both intracellular Ca^{2+} release and sarcolemmal ionic currents [43]. Recent studies have suggested that spontaneous Ca^{2+} release from the SR is an important mechanism of automaticity [44,45]. Indeed, spontaneous rhythmic Ca^{2+} release from the SR in pacemaker cells results in an increase in $[Ca^{2+}]_i$, which in turn activates I_{NCX} and leads to membrane depolarization [46,47]. To date, no clear mechanism has been discovered that shows how T-VDCC regulates cardiac automaticity. However, the present study showed that STIM1 is a key element in a previously unknown mechanism for regulating T-VDCC activity, suggesting that it may contribute to modulate the cardiac rhythmicity and excitability of native pacemaker cells.

We found that HL-1 cells display mostly $I_{Ca,T}$, which is in agreement with previous reports showing that the predominant Ca^{2+} current in HL-1 cells is mediated by T-VDCC [26]. Two previous studies reported that the depletion of the Ca^{2+} store negatively regulates L-VDCC activity in A7r5 cells, T-lymphocytes, and primary cortical neurons [48,49]. The overexpression of STIM1 or the expression of a STIM1 EF-hand mutant unable to detect Ca^{2+} in the SR both reduced the

function of endogenous L-VDCC [48,49]. These studies also showed that STIM1 directly interacts with $Ca_V1.2$ and inhibits its activity. While our results do not rule out the involvement of L-VDCC in the contraction of HL-1 cells, they strongly suggest that STIM1 directly regulates T-VDCC. Indeed, we showed that STIM1 co-immunoprecipitates with T-VDCC and that knocking down STIM1 increases $I_{Ca,T}$ density without affecting its availability, suggesting that STIM1 may play a role in the expression of T-VDCC. To corroborate this hypothesis, we showed that knocking down STIM1 also increased T-VDCC surface expression. Further studies are needed to evaluate the exact role of STIM1 in T-VDCC trafficking. Our study, together with the studies of Park et al. [48] and Wang et al. [49], describe a new role for STIM1 in excitable cells. Contrary to its main role in non-excitable cells which is to detect Ca^{2+} levels in the ER in order to replenish it, in excitable cells STIM1 physically interacts with VDCC to prevent an excessive Ca^{2+} entry into the cell by reducing VDCC surface expression. Further studies are needed to determine whether the exact mechanism underlying the cell surface expression of T-VDCC is dependent on the Ca^{2+} content of the SR or on the expression and localization of STIM1. Thus, in atrial myocytes, in which the SERCA pump is abundantly expressed, the negative regulation of Ca^{2+} entry may be an important mechanism for preventing Ca^{2+} overload and arrhythmogenic events. This idea is supported by our results showing that caffeine-induced Ca^{2+} release was significantly higher in cells transfected with siSTIM1.

In conclusion, our results suggest that STIM1 negatively regulates T-VDCC activity in HL-1 cells by reducing its cell surface expression, thus preventing an SR Ca^{2+} overload that can elicit arrhythmogenic events.

Supplementary data to this article can be found online at http://dx.doi.org/10.1016/j.bbamcr.2013.02.027.

Sources of funding

This work was supported by the Heart & Stroke Foundation of Quebec (G.G. and G.B.); the Canadian Institutes of Health Research (R.D., G.G. and G.B.); and the Natural Sciences and Engineering Research Council of Canada (M.G.).

Conflict of interest

None declared.

Acknowledgements

We want to thank Yannick Miron for technical assistance with the contraction assays.

References

[1] N. Frey, T. McKinsey, E. Olson, Decoding calcium signals involved in cardiac growth and function, Nat. Med. 6 (2000) 1221–1227.
[2] A. Fabiato, Calcium-induced release of calcium from the cardiac sarcoplasmic reticulum, Am. J. Physiol. Cell Physiol. 245 (1983) C1–C14.
[3] J. Stiber, A. Hawkins, Z. Zhang, S. Wang, J. Burch, V. Graham, C. Ward, M. Seth, E. Finch, N. Malouf, R. Williams, J. Eu, P. Rosenberg, STIM1 signalling controls store-operated calcium entry required for development and contractile function in skeletal muscle, Nat. Cell Biol. 10 (2008) 688–697.
[4] T. Ohba, H. Watanabe, M. Murakami, T. Sato, K. Ono, H. Ito, Essential role of STIM1 in the development of cardiomyocyte hypertrophy, Biochem. Biophys. Res. Commun. 389 (2009) 172–176.
[5] M. Voelkers, M. Salz, N. Herzog, D. Frank, N. Dolatabadi, N. Frey, N. Gude, O. Friedrich, W. Koch, H. Katus, M. Sussman, P. Most, Orai1 and Stim1 regulates normal and hypertrophic growth in cardiomyocytes, J. Mol. Cell. Cardiol. 48 (2010) 1329–1334.
[6] J. Roos, P. DiGregorio, A. Yeromin, K. Ohlsen, M. Lioudyno, S. Zhang, O. Safrina, J. Kozak, S. Wagner, M. Cahalan, G. Veliçelebi, K. Stauderman, STIM1, an essential and conserved component of store-operated Ca^{2+} channel function, J. Cell Biol. 169 (2005) 435–445.
[7] M. Vig, C. Peinelt, A. Beck, D.L. Koomoa, D. Rabah, M. Koblan-Huberson, S. Kraft, H. Turner, A. Fleig, R. Penner, J.P. Kinet, CRACM1 is a plasma membrane protein essential for store-operated Ca^{2+} entry, Science 312 (2006) 1220–1223.
[8] J. Liou, M.L. Kim, W.D. Heo, J.T. Jones, J.W. Myers, J.E. Ferrell, T. Meyer, STIM is a Ca^{2+} sensor essential for Ca^{2+}-store-depletion-triggered Ca^{2+} influx, Curr. Biol. 15 (2005) 1235–1241.
[9] S. Zhang, Y. Yu, J. Roos, J. Kozak, T. Deerinck, M. Ellisman, K. Stauderman, M. Cahalan, STIM1 is a Ca^{2+} sensor that activates CRAC channels and migrates from the Ca^{2+} store to the plasma membrane, Nature 437 (2005) 902–905.
[10] J. Liou, M. Fivaz, T. Inoue, T. Meyer, Live-cell imaging reveals sequential oligomerization and local plasma membrane targeting of stromal interaction molecule 1 after Ca^{2+} store depletion, Proc. Natl. Acad. Sci. U. S. A. 104 (2007) 9301–9306.
[11] M.M. Wu, J. Buchanan, R.M. Luik, R.S. Lewis, Ca^{2+} store depletion causes STIM1 to accumulate in ER regions closely associated with the plasma membrane, J. Cell Biol. 174 (2006) 803–813.
[12] A. Penna, A. Demuro, A. Yeromin, S. Zhang, O. Safrina, I. Parker, M. Cahalan, The CRAC channel consists of a tetramer formed by STIM-induced dimerization of Orai dimers, Nature 456 (2008) 116–120.
[13] S. Feske, Y. Gwack, M. Prakriya, S. Srikanth, S.H. Puppel, B. Tanasa, P.G. Hogan, R.S. Lewis, M. Daly, A. Rao, A mutation in Orai1 causes immune deficiency by abrogating CRAC channel function, Nature 441 (2006) 179–185.
[14] M. Prakriya, S. Feske, Y. Gwack, S. Srikanth, A. Rao, P.G. Hogan, Orai1 is an essential pore subunit of the CRAC channel, Nature 443 (2006) 230–233.
[15] C.D. Touchberry, C.J. Elmore, T.M. Nguyen, J.J. Andresen, X. Zhao, M. Orange, N. Weisleder, M. Brotto, W.C. Claycomb, M.J. Wacker, Store-operated calcium entry is present in HL-1 cardiomyocytes and contributes to resting calcium, Biochem. Biophys. Res. Commun. 416 (2011) 45–50.
[16] W. Claycomb, N.J. Lanson, B. Stallworth, D. Egeland, J. Delcarpio, A. Bahinski, N.J. Izzo, HL-1 cells: a cardiac muscle cell line that contracts and retains phenotypic characteristics of the adult cardiomyocyte, Proc. Natl. Acad. Sci. U. S. A. 95 (1998) 2979–2984.
[17] S. Cayouette, S.M. Bousquet, N. Francoeur, E. Dupré, M. Monet, H. Gagnon, Y.B. Guedri, C. Lavoie, G. Boulay, Involvement of Rab9 and Rab11 in the intracellular trafficking of TRPC6, Biochim. Biophys. Acta 1803 (2010) 805–812.
[18] X. Zhu, P.B. Chu, M. Peyton, L. Birnbaumer, Molecular-cloning of a widely expressed human homolog for the drosophila trp gene, FEBS Lett. 373 (1995) 193–198.
[19] G. Grynkiewicz, M. Poenie, R. Tsien, A new generation of Ca^{2+} indicators with greatly improved fluorescence properties, J. Biol. Chem. 260 (1985) 3440–3450.
[20] J. Domke, W. Parak, M. George, H. Gaub, M. Radmacher, Mapping the mechanical pulse of single cardiomyocytes with the atomic force microscope, Eur. Biophys. J. 28 (1999) 179–186.
[21] J.L. Hutter, J. Bechhoefer, Calibration of atomic-force microscope tips, Rev. Sci. Instrum. 64 (1993) 1868–1874.
[22] H.-J. Butt, M. Jaschke, Calculation of thermal noise in atomic force microscopy, Nanotechnology 6 (1995) 1–7.
[23] J.D. Levine, P. Funes, H.B. Dowse, J.C. Hall, Signal analysis of behavioral and molecular cycles, BMC Neurosci. 3 (2002) 1.
[24] A.V. Maltsev, V.A. Maltsev, M. Mikheev, L.A. Maltseva, S.G. Sirenko, E.G. Lakatta, M.D. Stern, Synchronization of stochastic Ca^{2+} release units creates a rhythmic Ca^{2+} clock in cardiac pacemaker cells, Biophys. J. 100 (2011) 271–283.
[25] S. White, P. Constantin, W. Claycomb, Cardiac physiology at the cellular level: use of cultured HL-1 cardiomyocytes for studies of cardiac muscle cell structure and function, Am. J. Physiol. Heart Circ. Physiol. 286 (2004) H823–H829.
[26] M. Xia, J.J. Salata, D.J. Figueroa, A.M. Lawlor, H.A. Liang, Y. Liu, T.M. Connolly, Functional expression of L- and T-type Ca^{2+} channels in murine HL-1 cells, J. Mol. Cell. Cardiol. 36 (2004) 111–119.
[27] Y. Hirano, A. Moscucci, C.T. January, Direct measurement of L-type Ca^{2+} window current in heart cells, Circ. Res. 70 (1992) 445–455.
[28] A.L. Hodgkin, A.F. Huxley, A quantitative description of membrane current and its application to conduction and excitation in nerve, J. Physiol. 117 (1952) 500–544.
[29] J. Satin, L.L. Cribbs, Identification of a T-type Ca^{2+} channel isoform in murine atrial myocytes (AT-1 cells), Circ. Res. 86 (2000) 636–642.
[30] J.S. Hulot, J. Fauconnier, D. Ramanujam, A. Chaanine, F. Aubart, Y. Sassi, S. Merkle, O. Cazorla, A. Ouillé, M. Dupuis, L. Hadri, D. Jeong, S. Mühlstedt, J. Schmitt, A. Braun, L. Bénard, Y. Saliba, B. Laggerbauer, B. Nieswandt, A. Lacampagne, R.J. Hajjar, A.M. Lompré, S. Engelhardt, Critical role for stromal interaction molecule 1 in cardiac hypertrophy, Circulation 124 (2011) 796–805.
[31] X. Luo, B. Hojayev, N. Jiang, Z.V. Wang, S. Tandan, A. Rakalin, B.A. Rothermel, T.G. Gillette, J.A. Hill, STIM1-dependent store-operated Ca^{2+} entry is required for pathological cardiac hypertrophy, J. Mol. Cell. Cardiol. 52 (2012) 136–147.
[32] M.D. Cahalan, STIMulating store-operated Ca^{2+} entry, Nat. Cell Biol. 11 (2009) 669–677.
[33] P. Varnai, L. Hunyady, T. Balla, STIM and Orai: the long-awaited constituents of store-operated calcium entry, Trends Pharmacol. Sci. 30 (2009) 118–128.
[34] R.S. Lewis, Store-operated calcium channels: new perspectives on mechanism and function, Cold Spring Harb. Perspect. Biol. 3 (2011) a003970.
[35] W.T. Clusin, Calcium and cardiac arrhythmias: DADs, EADs, and alternans, Crit. Rev. Clin. Lab. Sci. 40 (2003) 337–375.
[36] M.J. Janse, A.A. Wilde, Molecular mechanisms of arrhythmias, Rev. Port. Cardiol. 17 (Suppl. 2) (1998) 41–46.
[37] M.E. Diaz, H.K. Graham, S.C. O'Neill, A.W. Trafford, D.A. Eisner, The control of sarcoplasmic reticulum Ca content in cardiac muscle, Cell Calcium 38 (2005) 391–396.
[38] H. Cheng, W. Lederer, M. Cannell, Calcium sparks: elementary events underlying excitation–contraction coupling in heart muscle, Science 262 (1993) 740–744.
[39] S.L. Lipsius, J. Hüser, L.A. Blatter, Intracellular Ca^{2+} release sparks atrial pacemaker activity, News Physiol. Sci. 16 (2001) 101–106.
[40] C.I. Spencer, J.S. Sham, Effects of Na^+/Ca^{2+} exchange induced by SR Ca^{2+} release on action potentials and afterdepolarizations in guinea pig ventricular myocytes, Am. J. Physiol. Heart Circ. Physiol. 285 (2003) H2552–H2562.

[41] Z. Zhou, S.L. Lipsius, T-type calcium current in latent pacemaker cells isolated from cat right atrium, J. Mol. Cell. Cardiol. 26 (1994) 1211–1219.
[42] J. Hüser, L.A. Blatter, S.L. Lipsius, Intracellular Ca^{2+} release contributes to automaticity in cat atrial pacemaker cells, J. Physiol. 524 (Pt 2) (2000) 415–422.
[43] Z. Yang, K.T. Murray, Ionic mechanisms of pacemaker activity in spontaneously contracting atrial HL-1 cells, J. Cardiovasc. Pharmacol. 57 (2011) 28–36.
[44] V.A. Maltsev, E.G. Lakatta, Dynamic interactions of an intracellular Ca^{2+} clock and membrane ion channel clock underlie robust initiation and regulation of cardiac pacemaker function, Cardiovasc. Res. 77 (2008) 274–284.
[45] E.G. Lakatta, T.M. Vinogradova, V.A. Maltsev, The missing link in the mystery of normal automaticity of cardiac pacemaker cells, Ann. N. Y. Acad. Sci. 1123 (2008) 41–57.
[46] K.Y. Bogdanov, T.M. Vinogradova, E.G. Lakatta, Sinoatrial nodal cell ryanodine receptor and Na^{+}-Ca^{2+} exchanger: molecular partners in pacemaker regulation, Circ. Res. 88 (2001) 1254–1258.
[47] T.M. Vinogradova, V.A. Maltsev, K.Y. Bogdanov, A.E. Lyashkov, E.G. Lakatta, Rhythmic Ca^{2+} oscillations drive sinoatrial nodal cell pacemaker function to make the heart tick, Ann. N. Y. Acad. Sci. 1047 (2005) 138–156.
[48] C.Y. Park, A. Shcheglovitov, R. Dolmetsch, The CRAC channel activator STIM1 binds and inhibits L-type voltage-gated calcium channels, Science 330 (2010) 101–105.
[49] Y. Wang, X. Deng, S. Mancarella, E. Hendron, S. Eguchi, J. Soboloff, X.D. Tang, D.L. Gill, The calcium store sensor, STIM1, reciprocally controls Orai and $Ca_V1.2$ channels, Science 330 (2010) 105–109.